DYNAMIC PERFORMANCE OF NON-CIRCULAR GAS BEARINGS

S. S. WADHWA, R. SINHASAN and D. V. SINGH
University of Roorkee, ROORKEE-27672 INDIA

Received September 14, 1983
Presented by Prof. Dr. László Varga

This paper presents the dynamic performance characteristics of elliptical and three-lobe gas bearings. The perturbation formulation suggested by Lund has been modified to obtain stiffness and damping properties. Stability studies have been carried out for selected compressibility parameters. Comparison of performance characteristics of both types of bearings has been made.

Nomenclature

B_{jk} — $\bar{B}_{jk}C\vartheta/p_aR^2$, damping coefficients (dimensionless)
$\bar{B}_{jk}$ — damping coefficients ($j=1,2$; $k=1,2$)
C_R — C/R' clearance (dimensionless)
C — bearing clearance
$\bar{e}$ — eccentricity
h — $\bar{h}/C'$ film thickness (dimensionless)
$\bar{h}$ — film thickness
h_0 — film thickness in static equilibrium (dimensionless)
L — bearing length
M — $\bar{M}C\vartheta^2/p_aR^2$, journal mass (dimensionless)
$\bar{M}$ — journal mass
M_J — $\bar{M}_JC\vartheta^2/p_aR^2$, critical mass (dimensionless)
$\bar{M}_J$ — critical mass
N_i, N_j — shape functions ($i=1,4$; $j=1,4$)
0_b — bearing centre
0_j — journal centre
p — $\bar{p}/p_a$, pressure (dimensionless)
$\bar{p}$ — pressure
p_a — ambient pressure
p_0 — pressure in static equilibrium (dimensionless)
q_s — flow across the boundary of element

q_x, q_y — $\bar{q}_x/C$, $\bar{q}_y/C$: coordinates of displacement of journal centre (dimensionless)
$\bar{q}_x$, $\bar{q}_y$ — displacements along x and y directions
R — bearing radius
S_m — boundary of the mth element
S_{jk} — $\bar{S}_{jk}C/p_aR^2$, stiffness coefficients (dimensionless)
$\bar{S}_{jk}$ — stiffness coefficients ($j=1,2$; $k=1,2$)
W_0 — $\bar{W}_0/p_aR^2$, film force in static equilibrium (dimensionless)
$\bar{W}_0$ — film force in static equilibrium
x, y, z — bearing fixed orthogonal axes
x_B, y_B — coordinates of centre of curvature of bearing surface
x_J, y_J — coordinates of journal centre
ω — angular speed of rotation
ε — $\bar{e}/C$, bearing eccentricity (dimensionless)
ε_p — bearing ellipticity (dimensionless)
Λ — $\dfrac{6\mu\omega}{p_a}(R/C)^2$, compressibility parameter (dimensionless)
μ — viscosity
τ — $i\vartheta t$, time (dimensionless)
ϑ — whirl frequency
γ — $\dfrac{\vartheta}{\omega}$, frequency ratio (dimensionless)
Θ — angular coordinate measured from X — axis

Matrices

$[K]$ — fluidity matrix for entire assemblage
$\{p_1\}$, $\{p_2\}$ — nodal pressure for entire assemblage
$\{Q_1\}$, $\{Q_2\}$ — nodal flows for entire assemblage
$\{F_{w1}\}$, $\{F_{w2}\}$ — hydrodynamic terms for entire assemblage
$\{q\}$ — $\begin{Bmatrix} q_x \\ q_y \end{Bmatrix}$, coordinates of displacement of journal centre
$\{\dot{q}\}$ — $\dfrac{d}{d\tau}\{q\}$
$\{\ddot{q}\}$ — $\dfrac{d^2}{d\tau^2}\{q\}$

Introduction

The hydrodynamic gas bearings have the advantage of negligible friction losses, cleanliness and easy availability of air as lubricant but they encounter two familiar shortcomings, i.e., low load carrying capacity and hydrodynamic instability. Bearings of non-circular cross-section (Figs 1 and 2) using two or more circular lobes, permit large operating lobe eccentricity and still ensure minimum film thickness to avoid metal to metal contact. They are, therefore, capable of much superior dynamic performance [1] and partly overcome the problems associated with circular gas bearings.

The finite element method has been in use during the last one decade for obtaining solution to lubrication problems [2, 3]. Bulk of the work in this area, however, concerns the incompressible fluids and comparatively a small amount of literature [4, 5] using FEM techniques for solving lubrication problems for compressible fluids is available. Using the finite element method and modifying the perturbation formulation as suggested by Lund [6], this paper presents the dynamic properties of elliptical and three lobe gas bearings (Figs 1 and 2). The modified method is simpler and more straightforward than that earlier suggested by Lund. Stability studies have been carried out for selected compressibility parameters.

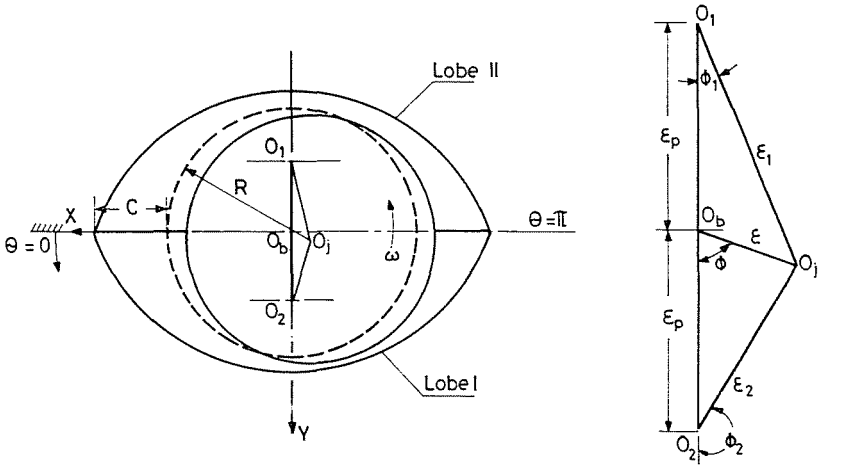

Fig. 1. Geometry of Elliptical Bearing

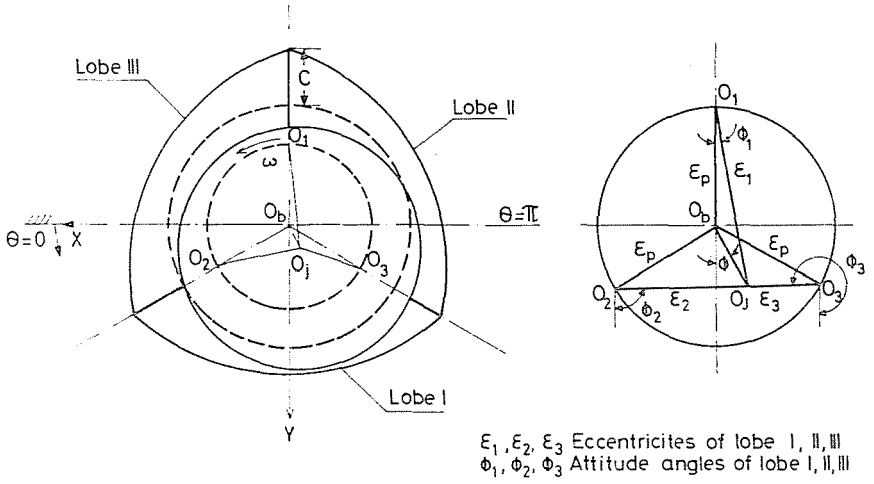

Fig. 2. Geometry of Three-Lobe Bearing

Theoretical Analysis and Finite Element Formulation

For compressible fluids and isothermal conditions, the Reynolds equation in non-dimensional form is,

$$\frac{\partial}{\partial\Theta}\left(h^3\frac{\partial p^2}{\partial\Theta}\right)+\frac{\partial}{\partial z}\left(h^3\frac{\partial p^2}{\partial z}\right)=2\Lambda\frac{\partial(ph)}{\partial\Theta}+i4\gamma\Lambda\frac{\partial(ph)}{\partial\tau}. \tag{1}$$

The film thickness is given by

$$h_0=1-(x_J-x_B)\cos\Theta-(y_J-y_B)\sin\Theta. \tag{2}$$

If the journal centre position is perturbed by δx_J and δy_J from its static equilibrium position identified by x_{J0} in horizontal and y_{J0} in vertical direction, the new position is given by

$$x_J=x_{J0}+\delta x_J$$

$$y_J=y_{J0}+\delta y_J.$$

Here, δx_J and δy_J are small and define harmonic motion in which

$$\delta x_J=\mathrm{Re}\{|\delta x_J|e^{\tau}\} \qquad \text{and} \qquad \delta y_J=\mathrm{Re}\{|\delta y_J|e^{\tau}\}.$$

The corresponding equations for the dimensionless film thickness and pressure in the perturbed state are,

$$h = h_0 + \delta x_J \cos\Theta + \delta y_J \sin\Theta \tag{3}$$

$$p = p_0 + \delta x_J p_1 + \delta y_J p_2 . \tag{4}$$

The developed bearing surface is discretised using isoparametric elements. Galerkin's technique is applied to Eq. (1) to obtain the following equation

$$\int\int \frac{\partial N_i}{\partial\Theta} h^3 p \frac{\partial p}{\partial\Theta} d\Theta\, dz + \int\int \frac{\partial N_i}{\partial z} h^3 p \frac{\partial p}{\partial z} d\Theta\, dz - \int\int \frac{\partial N_i}{\partial\Theta} \Lambda p h\, d\Theta\, dz +$$
$$+ \int\int \left[i\, 2\gamma\Lambda \frac{\partial(ph)}{\partial\tau} \right] N_i d\Theta\, dz - \left[\int \left(h^3 p \frac{\partial p}{\partial\Theta} dz \right) N_i + \int \left(h^3 p \frac{\partial p}{\partial z} d\Theta \right) N_i - \right.$$
$$\left. - \int (\Lambda p h\, d\Theta) N_i \right] = 0. \tag{5}$$

For static equilibrium this equation reduces to

$$\int\int \frac{\partial N_i}{\partial\Theta} h_0^3 p_0 \frac{\partial p_0}{\partial\Theta} d\Theta\, dz + \int\int \frac{\partial N_i}{\partial z} h_0^3 p_0 \frac{\partial p_0}{\partial z} d\Theta\, dz -$$
$$- \int\int \frac{\partial N_i}{\partial\Theta} \Lambda p_0 h_0\, d\Theta\, dz + 2 \int N_i q_s\, ds_m = 0. \tag{6}$$

Equation (5) is differentiated partially with respect to δx_J and δy_J to obtain the equations for p_1 and p_2.

$$\int\int h_0^3 p_0 \left(\frac{\partial N_i}{\partial\Theta} \cdot \frac{\partial N_j}{\partial\Theta} + \frac{\partial N_i}{\partial z} \cdot \frac{\partial N_j}{\partial z} \right) p_{1j} d\Theta\, dz +$$
$$+ \int\int h_0^3 \left(\frac{\partial N_i}{\partial\Theta} \frac{\partial p_0}{\partial\Theta} + \frac{\partial N_i}{\partial z} \frac{\partial p_0}{\partial z} \right) p_{1j} N_j\, d\Theta\, dz -$$
$$- \int\int h_0 \left(\frac{\partial N_i}{\partial\Theta} \Lambda - i 2\gamma\, \Lambda N_i \right) N_j p_{1j}\, d\Theta\, dz + 2 \int N_i q_s\, ds_m =$$
$$= - \int\int 3 h_0^2 \cos\Theta\, p_0 \left(\frac{\partial N_i}{\partial\Theta} \cdot \frac{\partial p_0}{\partial\Theta} + \frac{\partial N_i}{\partial z} \cdot \frac{\partial p_0}{\partial z} \right) d\Theta\, dz +$$
$$+ \int\int \frac{\partial N_i}{\partial\Theta} \Lambda p_0 \cos\Theta\, d\Theta\, dz - i \int\int 2\Lambda p_0 \cos\Theta\, N_i d\Theta\, dz. \tag{7}$$

$$\int\int h_0^3 p_0\left(\frac{\partial N_i}{\partial \Theta}\cdot\frac{\partial N_j}{\partial \Theta}+\frac{\partial N_i}{\partial z}\cdot\frac{\partial N_j}{\partial z}\right)p_{2j}d\Theta\,dz+$$

$$+\int\int h_0^3\left(\frac{\partial N_i}{\partial \Theta}\cdot\frac{\partial p_0}{\partial \Theta}+\frac{\partial N_i}{\partial z}\cdot\frac{\partial p_0}{\partial z}\right)p_{2j}N_j\,d\Theta\,dz-$$

$$-\int\int h_0\left(\frac{\partial N_i}{\partial \Theta}\Lambda-i2\gamma\,\Lambda N_i\right)N_j p_{2j}\,d\Theta\,dz+2\int N_i q_s\,ds_m=$$

$$=-\int\int 3h_0^2\sin\Theta\,p_0\left(\frac{\partial N_i}{\partial \Theta}\cdot\frac{\partial p_0}{\partial \Theta}+\frac{\partial N_i}{\partial z}\cdot\frac{\partial p_0}{\partial z}\right)d\Theta\,dz+$$

$$+\int\int\frac{\partial N_i}{\partial \Theta}\Lambda p_0\sin\Theta\,d\Theta\,dz-i\int\int 2\Lambda p_0\sin\Theta\,N_i d\Theta dz. \tag{8}$$

The boundary conditions are,

$$\begin{aligned}
&p_0=p_a \quad z=\pm L/D\\
&p_1=0 \quad \Theta=0,\pi,2\pi \text{ (for elliptical bearing)}\\
&p_2=0 \quad \Theta=\pi/6,5\pi/6,3\pi/2 \text{ (for three-lobe bearing)}
\end{aligned} \tag{9}$$

$$\left.\begin{aligned}
p_0(\Theta,z)&=p_0(\Theta+2\pi,z)\\
p_1(\Theta,z)&=p_1(\Theta+2\pi,z)\\
p_2(\Theta,z)&=p_2(\Theta+2\pi,z)
\end{aligned}\right\}0\le\Theta\le2\pi\,. \tag{10}$$

For an element m, Eqs (7) and (8) can be represented as,

$$\begin{aligned}
[K]^m\{p_1\}^m&=\{Q_1\}^m+\{F_{w1}\}^m\\
[K]^m\{p_2\}^m&=\{Q_2\}^m+\{F_{w2}\}^m.
\end{aligned} \tag{11}$$

Following the usual procedure of assembling the element equations, the system equations can be written as,

$$\begin{aligned}
[K]\{p_1\}&=\{Q_1\}+\{F_{w1}\}\\
[K]\{p_2\}&=\{Q_2\}+\{F_{w2}\}.
\end{aligned} \tag{12}$$

Dynamic Performance Characteristics

Stiffness and Damping Coefficients

The hydrodynamic forces are computed by integration of pressure components p_1 and p_2. The horizontal and vertical components of these forces are:

$$\begin{Bmatrix} F_x \\ F_y \end{Bmatrix} = \int_{-L/D}^{+L/D} \int_{0}^{2\pi} (p_0 - 1 + \delta x_J p_1 + \delta y_J p_2) \begin{Bmatrix} \cos\Theta \\ \sin\Theta \end{Bmatrix} d\Theta \, dz. \tag{13}$$

From this equation F_x and F_y can be expressed by first order Taylor series expansions in the neighborhood of the steady-state equilibrium position:

$$\begin{aligned} F_x &= F_{x0} + Z_{xx}\delta x_J + Z_{xy}\delta y_J \\ F_y &= F_{y0} + Z_{yx}\delta x_J + Z_{yy}\delta y_J . \end{aligned} \tag{14}$$

From Eqs (13) and (14) the following relations are obtained:

$$\begin{Bmatrix} F_{x0} \\ F_{y0} \end{Bmatrix} = \int_{-L/D}^{+L/D} \int_{0}^{2\pi} (p_0 - 1) \begin{Bmatrix} \cos\Theta \\ \sin\Theta \end{Bmatrix} d\Theta \, dz, \tag{15}$$

$$\begin{Bmatrix} Z_{xx} \\ Z_{xy} \end{Bmatrix} = \int_{-L/D}^{+L/D} \int_{0}^{2\pi} p_1 \begin{Bmatrix} \cos\Theta \\ \sin\Theta \end{Bmatrix} d\Theta \, dz, \tag{16}$$

$$\begin{Bmatrix} Z_{yx} \\ Z_{yy} \end{Bmatrix} = \int_{-L/D}^{+L/D} \int_{0}^{2\pi} p_2 \begin{Bmatrix} \cos\Theta \\ \sin\Theta \end{Bmatrix} d\Theta \, dz. \tag{17}$$

The coefficients Z_{xx}, Z_{xy}, Z_{yx}, and Z_{yy} are in complex form and are given as

$$\begin{bmatrix} Z_{xx} & Z_{xy} \\ Z_{yx} & Z_{yy} \end{bmatrix} = \begin{bmatrix} S_{11} & S_{12} \\ S_{21} & S_{22} \end{bmatrix} + i \begin{bmatrix} B_{11} & B_{12} \\ B_{21} & B_{22} \end{bmatrix}. \tag{18}$$

The coefficients S_{11}, S_{12}, S_{21} and S_{22} are called stiffness coefficients and are computed by integrating the real part of the film pressures p_1 and p_2. Similarly, coefficients B_{11}, B_{12}, B_{21} and B_{22} are the damping coefficients obtained by integrating imaginary parts of film pressures p_1 and p_2.

Equation of Motion and Threshold Speed

The equation of motion for the linearized system can be written as,

$$\begin{bmatrix} M & 0 \\ 0 & M \end{bmatrix} \{\ddot{q}\} + \begin{bmatrix} B_{11} & B_{12} \\ B_{21} & B_{22} \end{bmatrix} \{\dot{q}\} + \begin{bmatrix} S_{11} & S_{12} \\ S_{21} & S_{22} \end{bmatrix} \{q\} = \begin{Bmatrix} 0 \\ 0 \end{Bmatrix} \tag{19}$$

The stability studies have been made for the system using the linearized equation of motion (Eq. (19)) and the Routh's Criteria [7]. Since the stiffness and damping coefficients are dependent upon the whirl frequency, an iterative procedure as detailed in Section 4, was followed to compute the whirl frequency ratio. The critical mass and the threshold speed, above which the system becomes unstable, are then calculated.

Solution Method

Equation (6), which corresponds to the static equilibrium condition is non-linear and is solved by the finite element method using the incremental approach of Reddi and Chu [3]. The static equilibrium solution has been obtained for vertical load support by computing the equilibrium attitude angle through iteration. The pressure distribution corresponding to the static equilibrium condition is used in solving Eqs (7) and (8). The pressure components p_1 and p_2 obtained from the solution of Eq. (12) are used for computing hydrodynamic forces and the stiffness and damping coefficients.

The whirl frequency ratio satisfying the characteristic equation of the linearized equation of motion (Eq. (19)) has also been obtained using an iterative procedure (Fig. 3). The starting value of whirl frequency ratio is taken as 0.5 for which stiffness and damping coefficients are computed. These are substituted in the characteristic equation of Eq. (19) and a residue is obtained. Depending on the magnitude of the residue, a new value of whirl frequency ratio is selected and the process is repeated until the residue becomes sufficiently small (.001). The critical mass obtained corresponding to the whirl frequency ratio so arrived is used to compute the threshold speed above which the system becomes unstable.

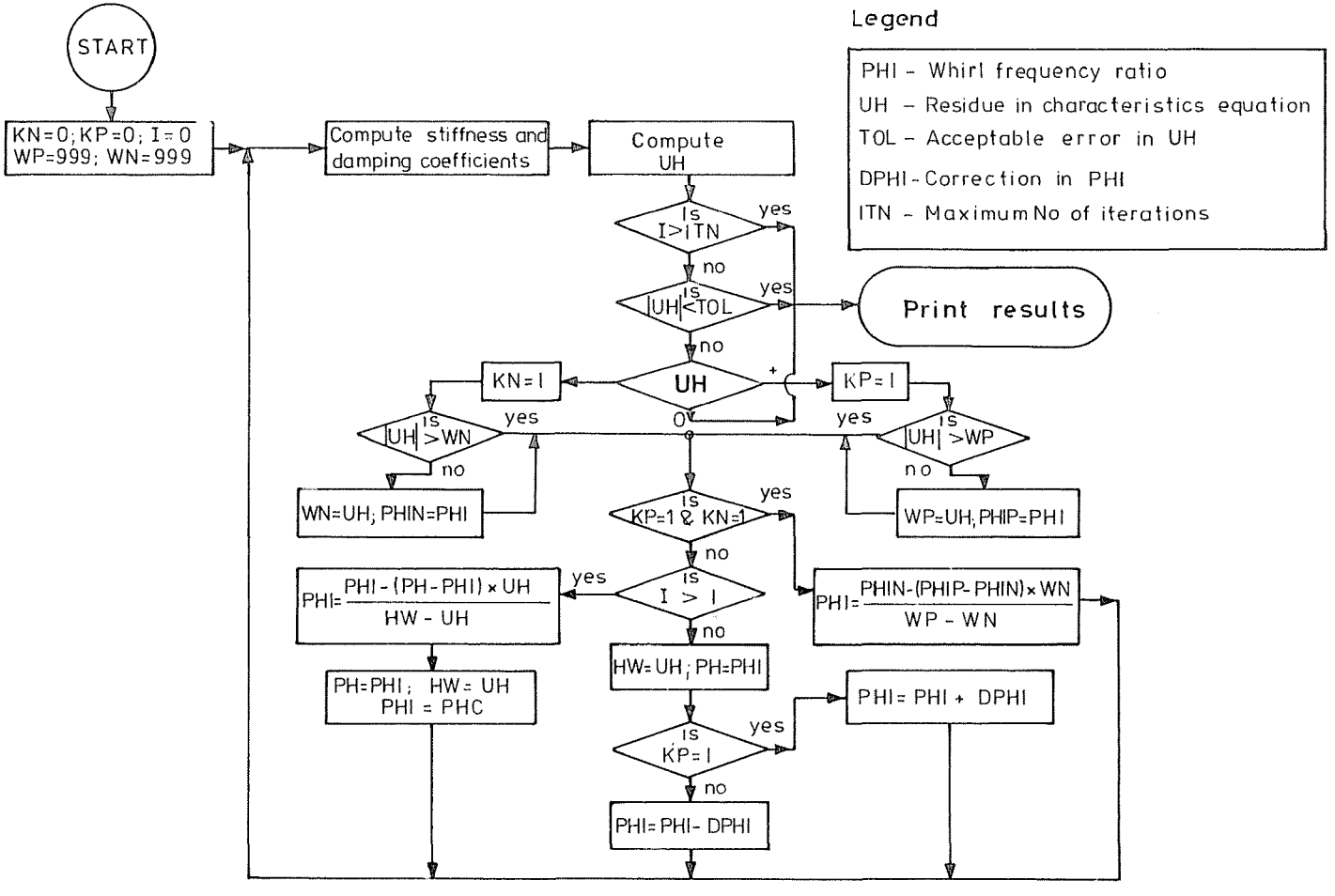

Fig. 3. Flow Diagram for Whirl Frequency Ratio

Results and Discussions

A computer program, based on the analysis of this paper, was developed to obtain the dynamic performance characteristics of elliptical and three-lobe bearings with compressible lubricant. The results obtained by the present method, using the finite element formulation, have been compared with those of Cheng [8] for the case of plane journal bearing. Figures 4 and 5 show the whirl frequency ratio and the threshold speed plotted against compressibility parameter (Λ). The results agree very well with those of Cheng for various compressibility parameters and bearing eccentricities.

The elliptical and three-lobe bearings studied in the present case have the same geometrical ($L/D=1$, $\varepsilon_p=0.5$) and operating parameters (ε, Λ) so that their performance characteristics can be compared.

The equilibrium attitude angles for vertical load support computed for elliptical and three-lobe bearings have been plotted in Figs 6 and 7. With the increase in the bearing eccentricity, the equilibrium attitude angle decreases. The rate of decrease is higher at larger values of the bearing eccentricity. It is also observed that at smaller values of the compressibility parameter, the three-lobe bearing has smaller equilibrium attitude angles, whereas at higher values of compressibility parameter, the elliptical bearing has lower equilibrium attitude angles. So, the nature of variations of attitude angles with eccentricity ratios and the compressibility parameter do not give a clear indication of the expected dynamic response of the elliptical bearing relative to that of the three-lobe bearing.

Stiffness and damping coefficients have been computed for half frequency whirl ($\gamma=0.5$) condition. For various bearing eccentricity ratios, these coefficients have been plotted against the compressibility parameter in Figs 8 to 23. The values of diagonal stiffness and damping coefficients (S_{11}, S_{22}, B_{11}, B_{22}) increase with increase in the compressibility parameter. The values of cross-coupling coefficients (S_{12}, S_{21}, B_{12} and B_{21}) start falling at higher compressibility parameters and eccentricity ratios. The stiffness and the damping coefficients do not follow a definite trend with regard to the two types of bearings.

Frequency ratios computed for various bearing eccentricity ratios and compressibility parameters, $\Lambda=1$ and 3, have been plotted in Figs 24 and 25. For both the compressibility parameters, the frequency ratios values decrease with the increase in bearing eccentricity ratios. For all the values of bearing eccentricity ratio, the elliptical bearing has higher values of frequency ratio at compressibility parameter, $\Lambda=1$ than those of the three-lobe bearing. On the

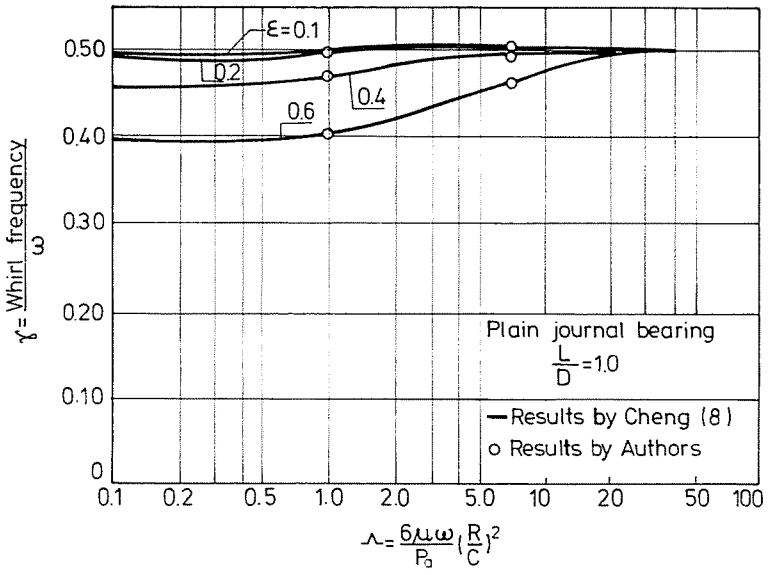

Fig. 4. Dimensionless Whirl Frequency

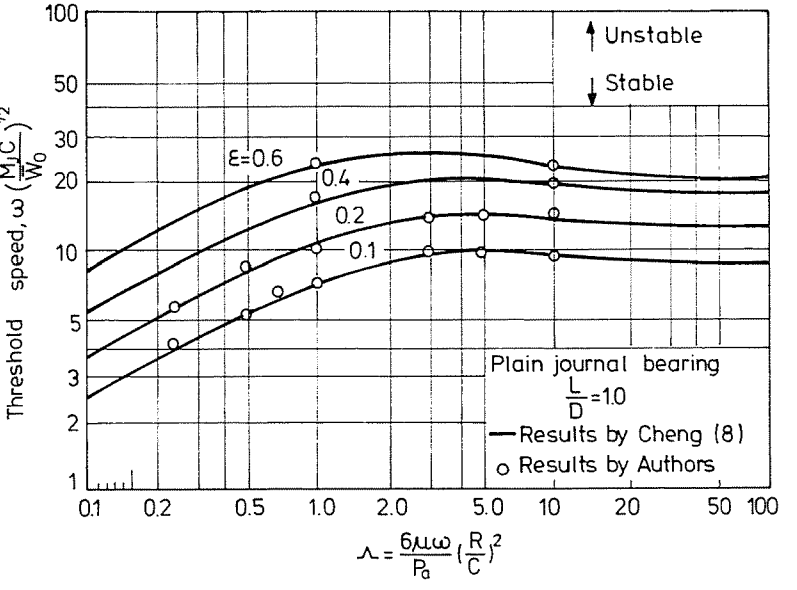

Fig. 5. Dimensionless Threshold Speed

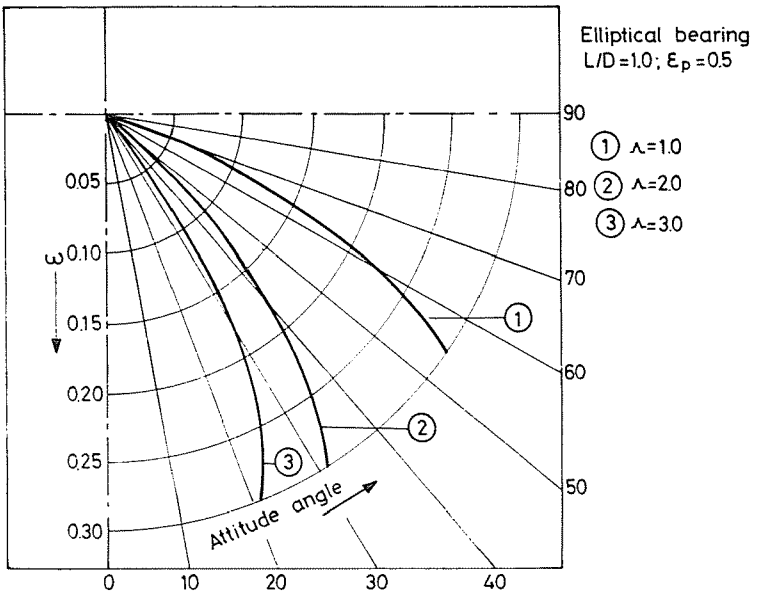

Fig. 6. Equilibrium Locus of Journal Centre for Vertical Load Support

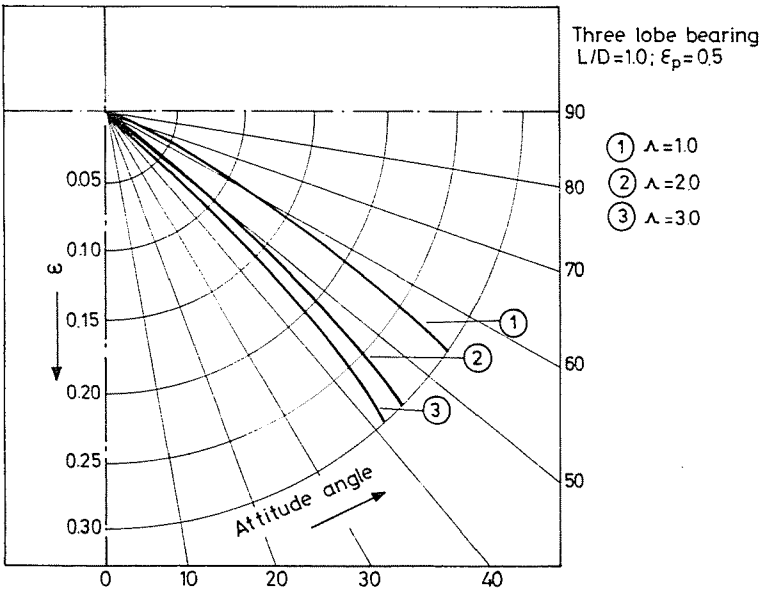

Fig. 7. Equilibrium Locus of Journal Centre for Vertical Load Support

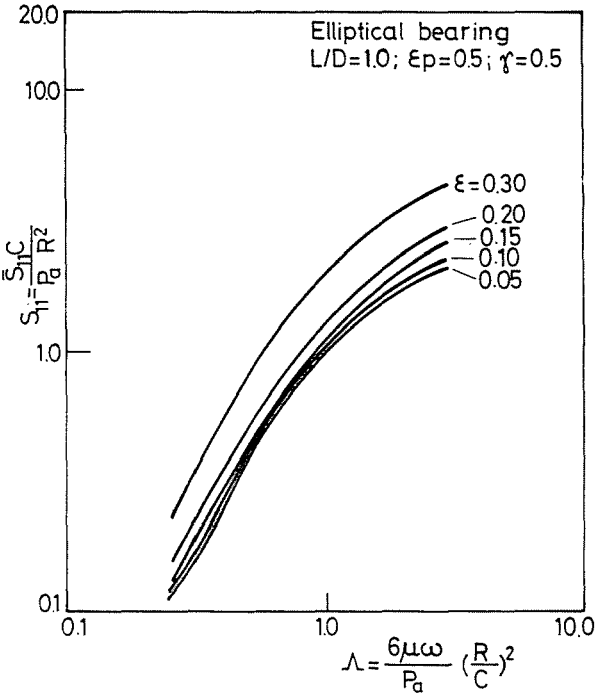

Fig. 8. Dimensionless Stiffness Coefficient, S_{11}

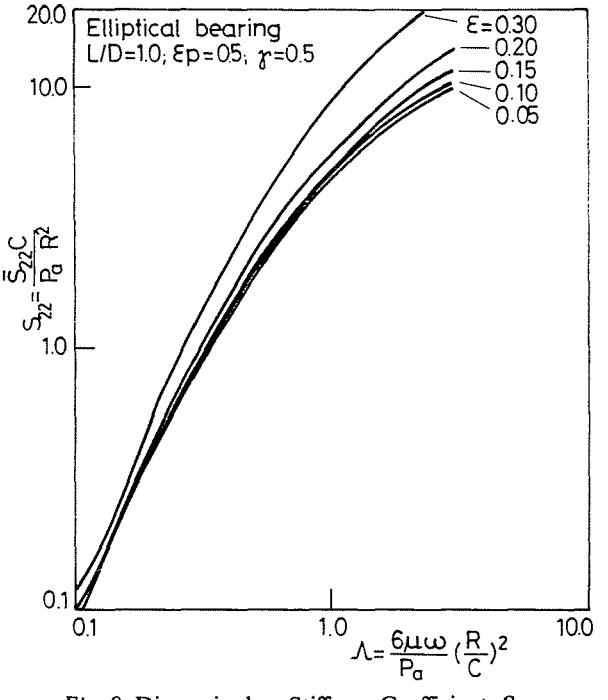

Fig. 9. Dimensionless Stiffness Coefficient, S_{22}

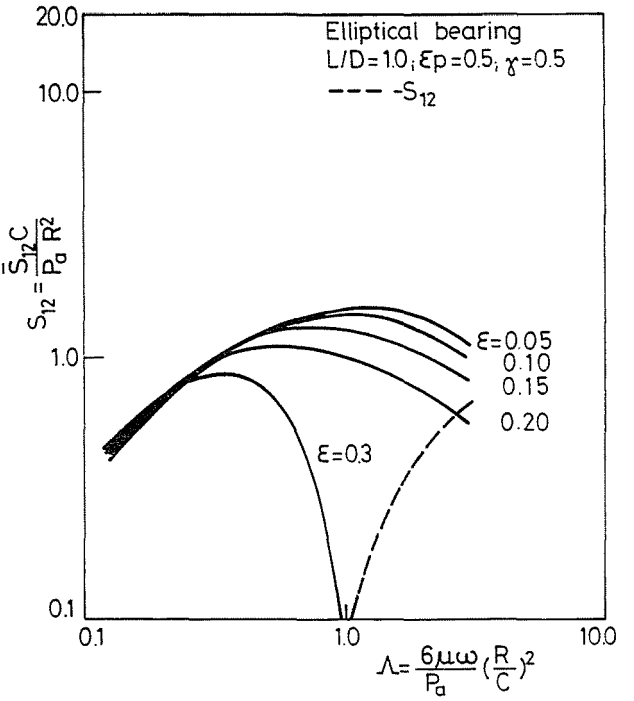

Fig. 10. Dimensionless Stiffness Coefficient, S_{12}

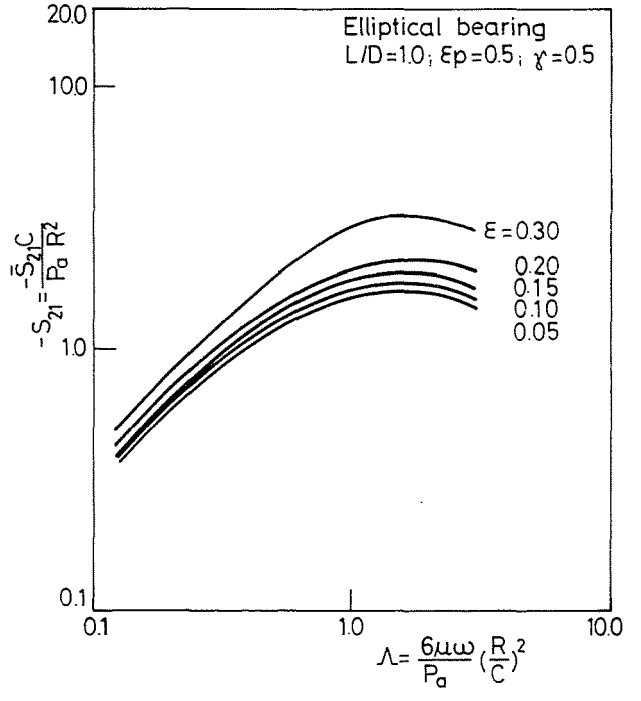

Fig. 11. Dimensionless Stiffness Coefficient, $-S_{21}$

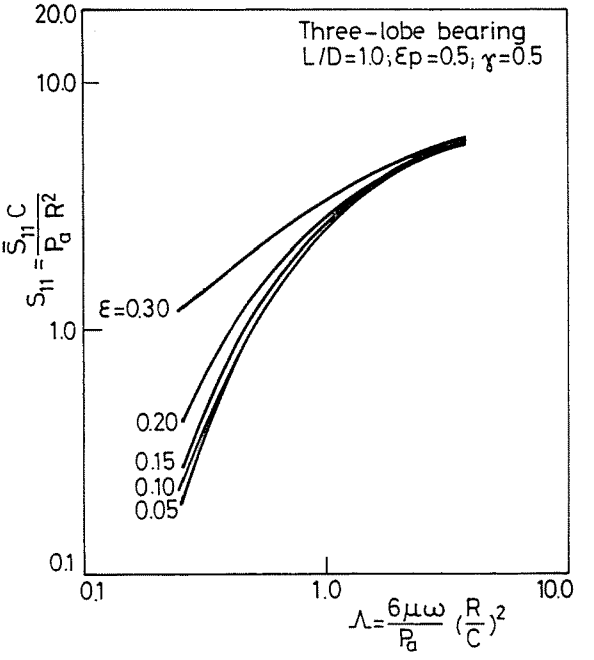

Fig. 12. Dimensionless Stiffness Coefficient, S_{11}

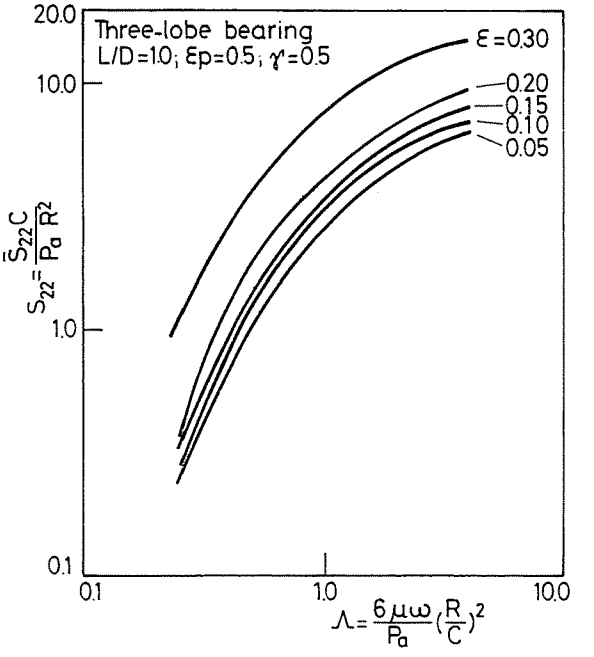

Fig. 13. Dimensionless Stiffness Coefficient, S_{22}

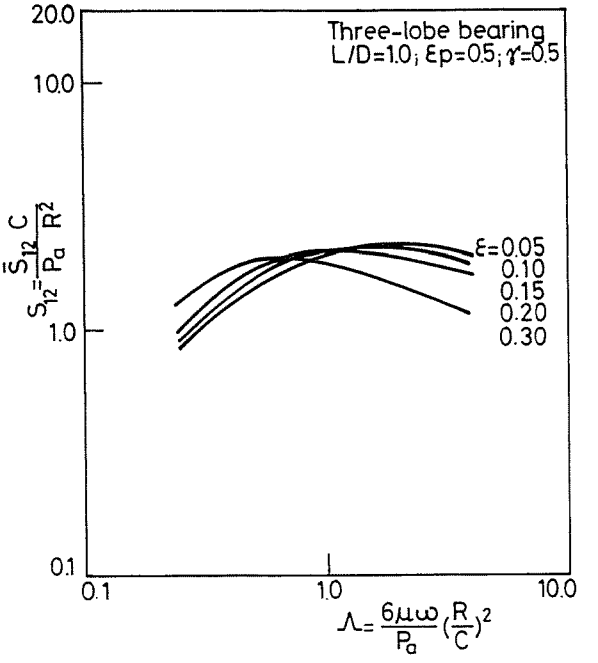

Fig. 14. Dimensionless Stiffness Coefficient, S_{12}

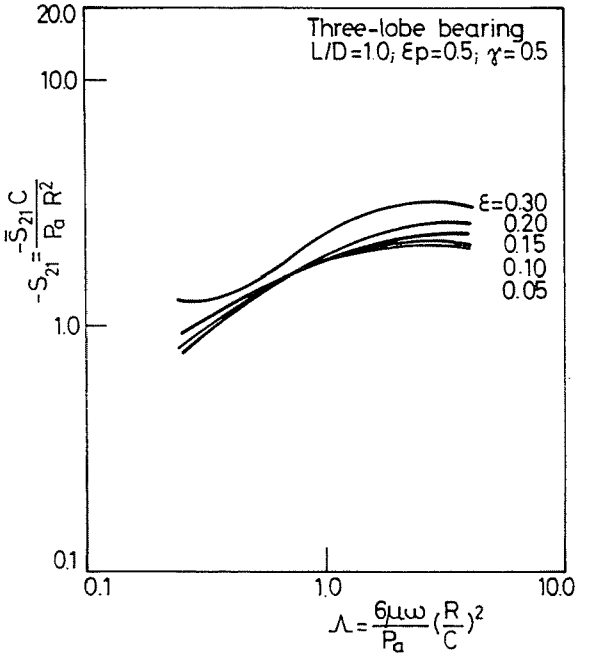

Fig. 15. Dimensionless Stiffness Coefficient, $-S_{21}$

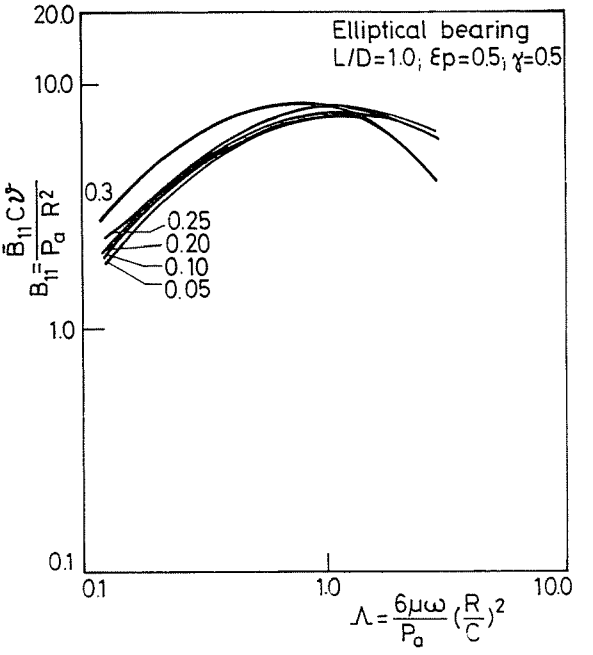

Fig. 16. Dimensionless Damping Coefficient, B_{11}

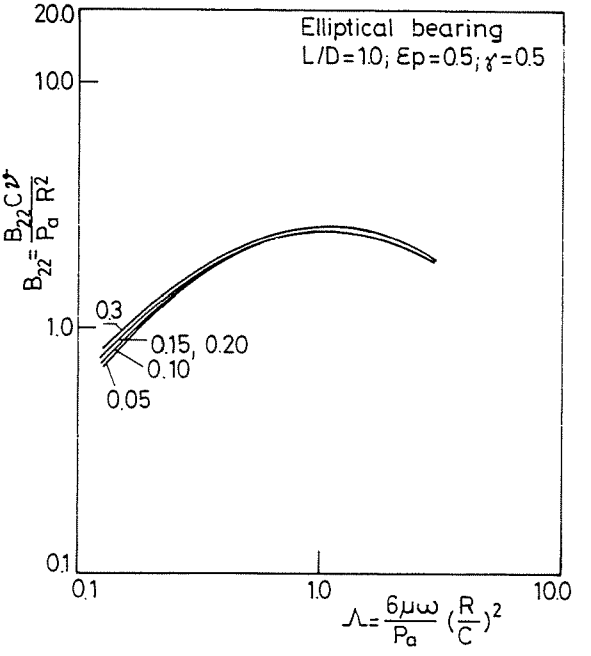

Fig. 17. Dimensionless Damping Coefficient, B_{22}

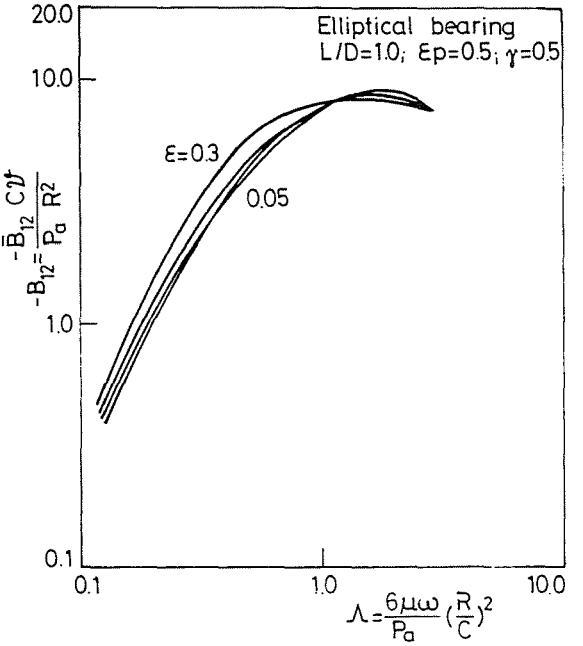

Fig. 18. Dimensionless Damping Coefficient, $-B_{12}$

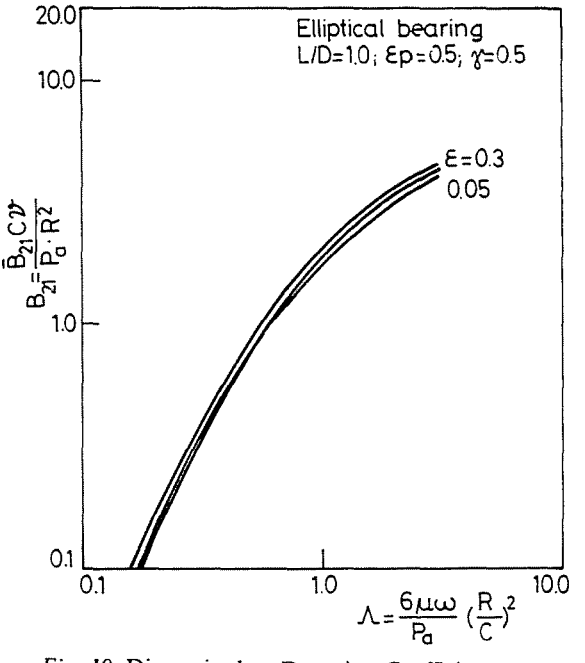

Fig. 19. Dimensionless Damping Coefficient, B_{21}

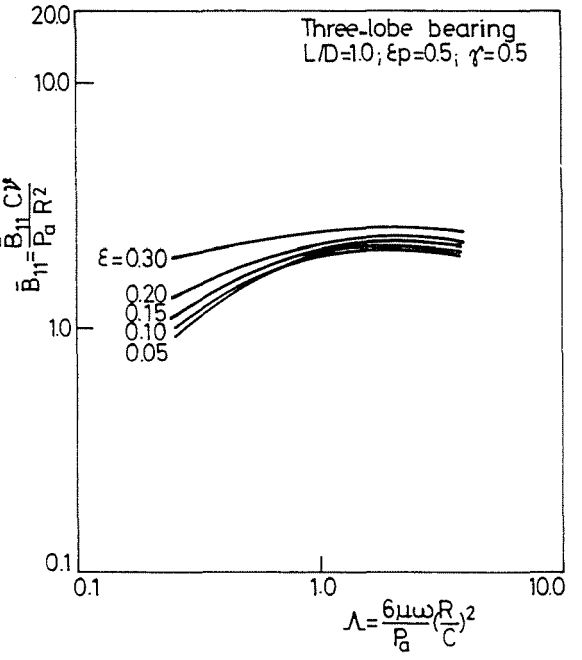

Fig. 20. Dimensionless Damping Coefficient, B_{11}

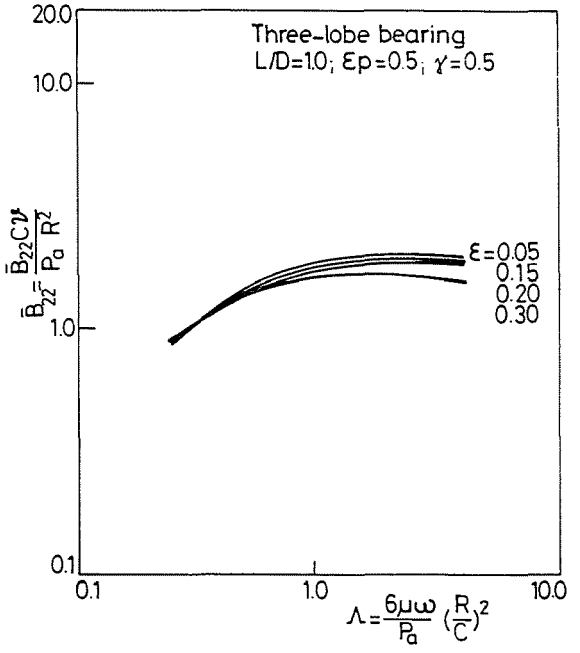

Fig. 21. Dimensionless Damping Coefficient, B_{22}

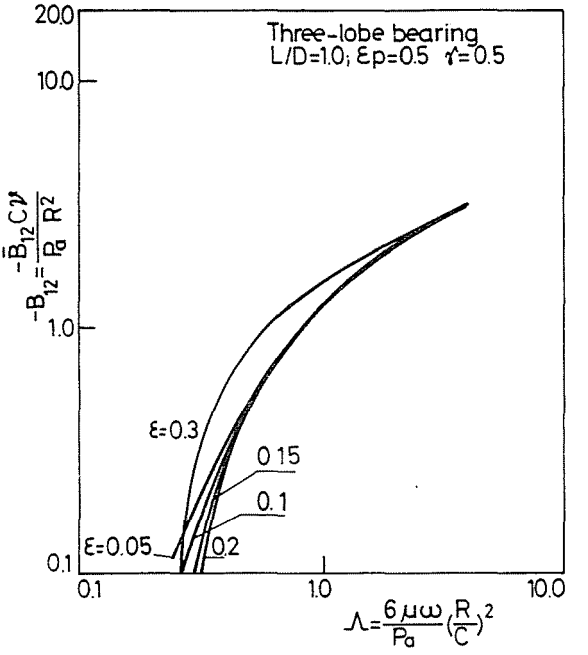

Fig. 22. Dimensionless Damping Coefficient, $-B_{12}$

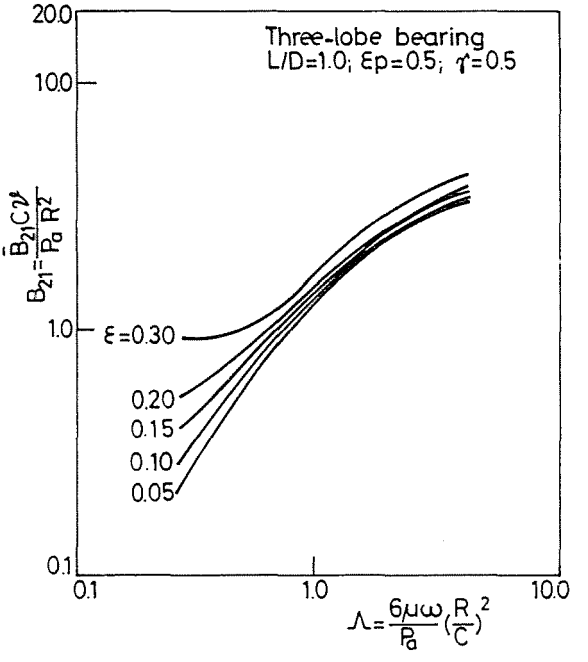

Fig. 23. Dimensionless Damping Coefficient, B_{21}

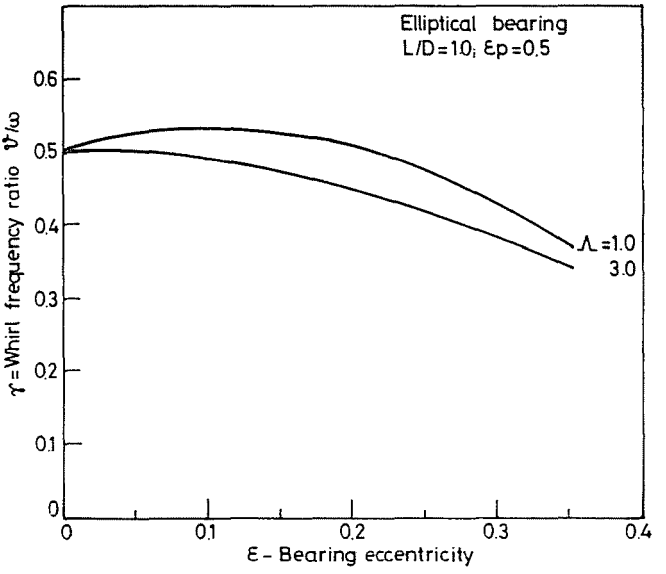

Fig. 24. Dimensionless Whirl Frequency Ratio

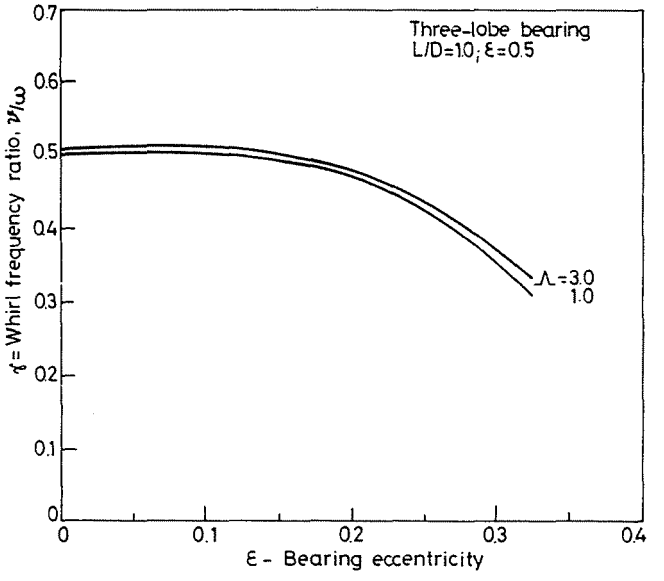

Fig. 25. Dimensionless Whirl Frequency Ratio

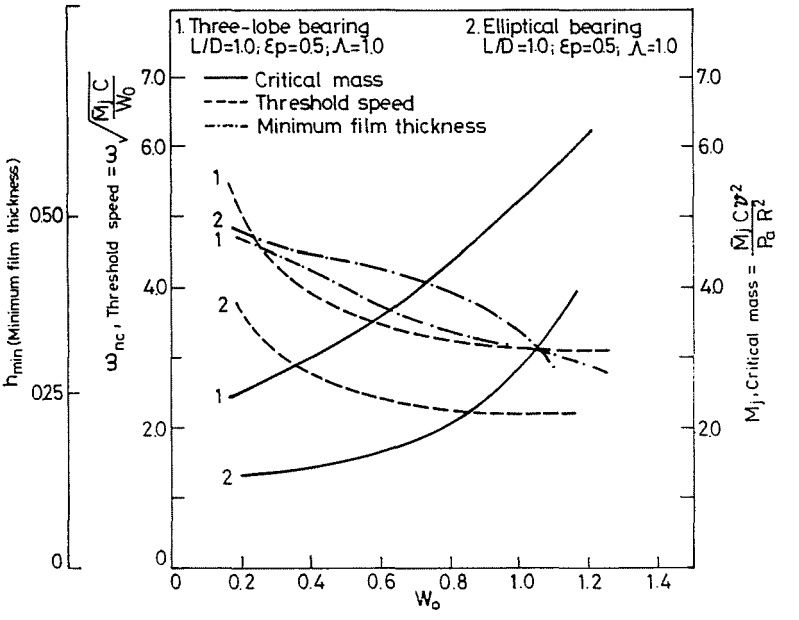

Fig. 26. Comparison of Stability of Elliptical and Three-Lobe Bearing

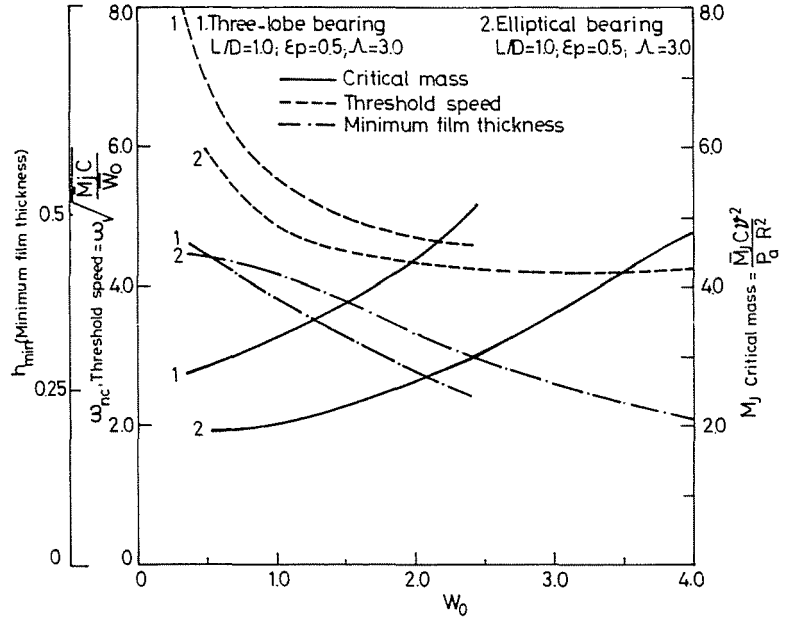

Fig. 27. Comparison of Stability of Elliptical and Three-Lobe Bearing

other hand, at $\Lambda = 3$, the three-lobe bearing has higher values of frequency ratio.

Critical mass, threshold speed and the minimum film thickness obtained for both types of bearings have been plotted against the load carrying capacity (W_0) in Figs 26 and 27. The critical mass values increase with the increase of the film force, whereas the threshold speed and minimum film thickness show a decreasing trend. Critical mass and threshold speed values are larger in the case of three-lobe bearing as compared to those for the elliptical bearing, for all the parameters studied, but the minimum film thickness is smaller.

It can therefore be concluded that for identical geometrical (L/D, ε_p) and operating (ε, Λ) parameters, the three-lobe bearing exhibits a larger domain of journal stability, but requires more exacting manufacturing tolerances.

References

1. PINKUS, O.: 'Analysis of Non-Circular Gas Journal Bearings', Trans. ASME, Jr. of Lubrication Technology, 616. (1975).
2. HUEBNER, K. H.: 'Finite Element Analysis of Fluid Film Lubrication — a Survey', Finite Elements in Fluids, Wiley, *2* 225. (1975).
3. BOOKER, J. F.—HUEBNER, K. H.: Application of Finite Element Method to Lubrication — an Engineering Approach, Trans. ASME, Jr. of Lubrication Technology, pp. 313—323. (1972).
4. REDDI, M. M.—CHU, T. Y.: Finite Element Solution of Steady State Compressible Lubrication Problems, Trans. ASME, Jr. of Lubrication Technology, pp. 495—503. (1970).
5. OH, K. P.—ROHDE, S. M.: A Theoretical Analysis of a Complient Shell Air Bearings, Jr. of Lubrication Technology, pp. 75—81. (1977).
6. LUND, J. W.: Calculations of Stiffness and Damping Properties of Gas Bearings, Trans. of ASME, Jr. of Lubrication Technology, pp. 793—803. (1968).
7. WILLIAM, J. L.: Stability Theory of Dynamical Systems, London, NELSON, (1970).
8. CHENG, H. S.—PAN, C. H. T.: Stability Analysis of Gas Lubricated, Self-acting, Plain, Cylindrical, Journal Bearings of Finite Length using Galerkin's Method, Jr. of Basic Engg. *87* 185. (1965).

S. S. WADHWA | Scientist, Central Building Research Institute, ROORKEE-24 7672 (INDIA)
R. SINHASAN, D. V. SINGH | Professor, Department of Mechanical and Industrial Engg., University of Roorkee, ROORKEE-24 7672 (INDIA)